High-resolution imaging diagnosis and staging of bladder cancer: comparison between optical coherence tomography and high-frequency ultrasound

Zhijia Yuan
Zhenguo Wang
Rubin Pan
SUNY at Stony Brook
Department of Biomedical Engineering
Stony Brook, New York 11794

Jingxuan Liu
SUNY at Stony Brook
Department of Pathology
Stony Brook, New York 11794

Harris Cohen
SUNY at Stony Brook
Department of Radiology
Stony Brook, New York 11794

Yingtian Pan
SUNY at Stony Brook
Department of Biomedical Engineering
Stony Brook, New York 11794

Abstract. A comparative study between 1.3-μm optical coherence tomography (OCT) and 40-MHz high-frequency ultrasound (HFUS) is presented to enhance imaging of bladder cancers *ex vivo*. A standard rat bladder cancer model in which transitional cell carcinoma (TCC) was induced by intravesical instillation of AY-27 cells was followed independently with both OCT and HFUS, and the image identifications were compared to histological confirmations. Results indicate that both OCT and HFUS were able to delineate the morphology of rat bladder [e.g., the urothelium (low backscattering/echo) and the underlying lamina propria and muscularis (high backscattering/echo]. OCT differentiated inflammatory lesions (e.g., edema, infiltrates and vasodilatation in lamina propria, hyperplasia) and TCC based on characterization of urothelial thickening and enhanced backscattering or heterogeneity (e.g., papillary features), which HFUS failed due to insufficient image resolution and contrast. On the other hand, HFUS was able to stage large T2 tumors that OCT failed due to limited imaging depth. The results suggest that multimodality cystoscopy combining OCT and HFUS may have the potential to enhance the diagnosis and staging of bladder cancers and to guide tumor resection, in which both high resolution ($\sim$10 μm) and enhanced penetration ($>$3mm) are desirable. © *2008 Society of Photo-Optical Instrumentation Engineers.* [DOI: 10.1117/1.2978059]

Keywords: optical coherence tomography; high-frequency ultrasound; bladder cancer; AY-27 cells.

Paper 07170RRR received May 10, 2007; revised manuscript received Apr. 7, 2008; accepted for publication Apr. 10, 2008; published online Sep. 12, 2008.

1 Introduction

Clinical statistics indicate that bladder cancer is the fifth most common cancer and the twelfth leading cause of cancer death in the U.S.[1] Bladder cancer is curable if detected and treated early. Therefore, an earlier and more accurate diagnosis is critical to the cure and therapeutic treatment of bladder cancer. Most bladder carcinoma originates in the thin basal cell layer of the urothelium, which is too thin to detect at its early stage by current medical imaging modalities, including intravenous X-ray and magnetic resonance imaging (MRI), noninvasive diagnosis of early bladder cancers remains a clinical challenge. Although current screening techniques, such as urine cytology,[2] fluorescence *in situ* hybridization,[3] and bladder cancer test (BTA)[4] have been routinely used in clinical detection of high-grade bladder malignancy, their sensitivity is insufficient to detect early low-grade cancers. Furthermore, a positive screening can be caused by floating cancer cells in the entire urinary tract; the lack of effective method to locate the cancerous lesions often compromises the ultimate effectiveness of these screening techniques. Because of this, symp-

tomatic patients are often followed by cystoscopy for visual inspection of superficial lesions on the bladder wall. However, almost all preclinical malignancies of bladder cancers (e.g., carcinoma *in situ*) demonstrates no significant gross lesions and are thus clinically unremarkable under cystoscopic examination. Because of the lack of depth resolution, cystoscopy is frequently followed by random biopsy for conclusive diagnosis and staging of bladder malignancy, which may miss early flat bladder cancers. Therefore, a noninvasive and high-resolution imaging technique is highly desirable to allow early diagnosis and more precise staging of bladder tumors.

Optical coherence tomography (OCT),[5] a fiber optically based imaging technique, is capable of visualizing tissue morphology at sub-10 μm axial resolution and to a depth of 2 to 3 mm below the tissue surface. Since its first introduction to ophthalmic imaging in the early 1990s, OCT has become an enabling noninvasive and high-resolution biomedical imaging modality that has found potential applications for the diagnosis of diseases in various biological tissues, including bladder cancers. Recent advances in OCT development include Doppler OCT to map subsurface blood flow,[6] polarization-sensitive OCT,[7] and spectroscopic OCT[8] to pro-

Address all correspondence to Yingtian Pan, SUNY at Stony Brook, Department of Biomedical Engineering, Stony Brook, New York 11794. Tel. 631-444-1451; Fax. 631-444-6646; E-mail: yingtian.pan@sunysb.edu

vide more specific image contrast and sensitivity, and spectral-domain OCT[9] to drastically enhance the frame rate for real-time 2-D and even 3-D *in vivo* imaging. The recently reported ultrahigh-resolution OCT (e.g., <1 μm axial resolution) by using ultrabroadband light source (e.g., ultrafast laser) has further demonstrated the potential for more precise diagnosis of early neoplasm.[10] Although our clinical study using MEMS endoscopic OCT[11] shows drastically enhanced diagnosis of bladder cancers, we have also noted that because of increased heterogeneity and blood-induced light attenuation within cancerous lesions OCT may not be able to provide sufficient imaging depth to stage bladder tumor invasion beyond stage T1 (invaded into lamina propria) or higher.

Parallel to OCT that detects the backscattering of light waves from the bladder wall, ultrasound imaging evaluation of the bladder can be performed noninvasively and quickly by detecting the backscattering of ultrasonic waves. Because of resolution limitations of transabdominal ultrasound imaging, the identification of morphological features pertinent to bladder cancers and progression has shown limited success for noninvasive detection in the clinic except for gross, outgrowing bladder tumors.[12] Transurethral ultrasound imaging has also been used in assessment of bladder tumor but is limited to the detection of large papillary tumors possibly due to insufficient resolution.[13] Recently, high-frequency ultrasound (HFUS) imaging has been applied for *in vivo* diagnosis and assessment of a variety of epithelial cancers.[14–16] Because of drastically improved resolution (e.g., ~ 40 μm for 40 MHz ultrasound), the delineation of some anatomic architectures, such as the lamina propria, the muscularis, and the fatty layer of the bladder wall, is permitted (under pseudocolor display), which may show the promise as a high-resolution imaging method for diagnosis and staging of bladder cancers. Although the resolution of HFUS is five to ten times lower than OCT, the penetration of HFUS can be extended from $1-3$ mm for OCT to $5-10$ mm, which is potentially very useful for the staging of bladder cancers. Larger field of view (FOV) of ultrasound is also an important advantage to image the entire bladder, which has a fairly large surface area. Furthermore, recent technological advances in both OCT and HFUS developments have permitted the integration into the endoscopes or catheters for high-resolution transurethral imaging diagnosis. Because of the similarities between these two imaging modalities, comparative studies of OCT and HFUS have been reported on imaging assessments of subsurface lesions, such as skin lesions,[17] GI tract,[18] and aortic plaques.[19] Here we present the first comparative study between 1.3 μm OCT and 40 MHz HFUS on bladder tissue imaging *ex vivo* and the results on the assessment of the utility and potential limitations of these two imaging modalities in the diagnosis and staging of bladder cancers based on a rat-bladder carcinogenesis model.

2 Method

A standard rat-bladder cancer model[20] was employed in which transitional cell carcinoma (TCC) was induced by intravesical instillation of AY-27 cells into the bladders of 39 female Fischer 344 rats. AY-27 cells, obtained from Dr. Selman's Lab at Ohio Medical College, were a cultured rat-bladder TCC cell line that was induced chemically from
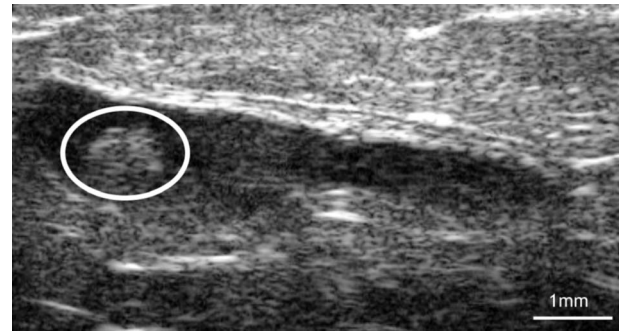
Fig. 1 *In vivo* trans-abdominal HFUS imaging of a $\sim$1 mm tumor as highlighted by a circle in a rat bladder on day 21 post-AY27 cell instillation.

N-(4-[5-nitro-2-furyl]-2-thiazolyl) formamide. The AY-27 cells from freezing stock were rapidly thawed in water bath at 38 $^\circ$C and grown in cell culture medium RPMI-1640 supplemented with 10% fetal calf serum and 2 mM L-glutamine, incubated at 37 $^\circ$C with humidified 5%-CO_2 and 95% airflow for cellular accumulation. After three to four days the subconfluent AY-27 cells were split and seeded onto more culture plates until sufficient cellular accumulation was reached. Then, the confluent AY-27 cells were detached from the plates by adding 0.1% trypsin, rinsed with phosphate buffered saline (PBS), centrifuged, and counted. The cells were resuspended at a concentration of 3×10^6/mL in the growth medium and maintained in a 37 $^\circ$C water bath; based on body weight (150 g/each), 0.15 mL of this cell suspension was to be instilled intravesically to yield $\sim 4.5 \times 10^5$ cells per rat bladder. The rats were anesthetized using inhalational 5% isoflurane for induction and 1–2.5% for maintenance, and maintained supinely on euthermic blanket. A xylocaine-coated sterile Tom Cat catheter was gently guided through the urethra and into the bladder of the rat to drain the urine prior to instillation. To facilitate tumor seeding, 0.15 mL of 0.1 mol/L HCl was instilled into the bladder for 15 s to mildly disrupt the urothelium and then neutralized with 0.15 mL 0.1 mol/L KOH for 15 s. The bladder was further drained and flushed two to three times with sterile PBS until pH 7.4. Subsequently, 0.15 mL of either 4.5×10^5 AY-27 cell suspension or sterile PBS (control) was instilled into the rat bladder and maintained for 1 hr, during which the rat was turned 90 deg every 15 min to expose the entire bladder to the instills evenly. After 1 hr, the catheter was removed and anesthesia was curtailed to allow the animal to void in cage.
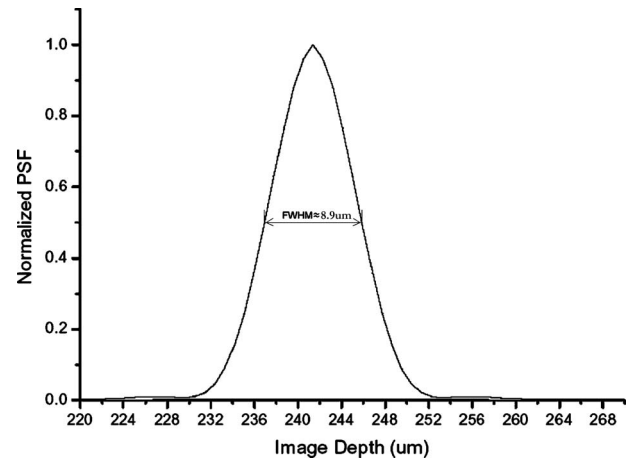
Studies indicated that TCCs routinely developed in rat bladders roughly between day 12 and 50;[20] therefore, *ex vivo* imaging studies were begun during days 10 to 30 to track daily the changes induced by tumorigenesis induced by AY-27 cell induction. However, it was found in our previous experiments that the TCC growth induced by this cancer model was not uniform; therefore, we performed *in vivo* trans-abdominal HFUS twice weekly after day 10 to track the onset of large TCCs, allowing us to effectively avoid papillary outburst and to determine the proper time course (i.e., from early to high-grade TCC) for final *ex vivo* study. For instance, Fig. 1 shows an *in vivo* HFUS image of a $\sim \phi 1$ mm tumor in the bladder on day 21. Prior to *ex vivo* imaging evaluation (end point),
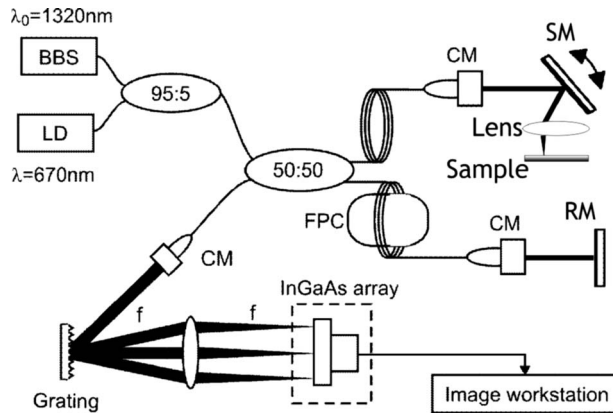
Fig. 2 Schematic of a fiberoptic spectral-domain OCT system. BBS: broadband source ($\lambda_0 = 1320$ nm, $\Delta\lambda_{FWHM} = 90$ nm, $P = 12$ mW); LD: aiming laser diode ($\lambda = 532$ nm); CM: fiberoptic collimator; FPC: fiber polarization controller; SM: scanning mirror; RM: reference mirror.

Fig. 3 Measured axial PSF of the SDOCT system. The measured axial resolution (~ 8.9 μm) is close to the theoretical coherence length of $L_c = 8.5$ μm.

both control and treated rats (blinded) were euthanized using anesthetic overdose and the intact bladder was removed by a midline laparotomy incision, opened from the urethra to the dome, and mounted uniformly on a ring holder placed in a modified Ringer's buffer solution (37 °C, pH 7.4) to undergo multiple OCT and HFUS scans *ex vivo*. Hematoxylin and eosin stained histology was performed on the sections precisely marked during OCT and HFUS scans to confirm the identifications of the image features made during imaging studies. All the animal experiments were conducted following the guidelines approved by the Institutional Animal Care and Use Committee of the Stony Brook University.

OCT operates analogously to ultrasound in that ultrasound detects time-lapse echoes of ultrasonic pulses whereas OCT detects pathlength-dependent backscattering (i.e., echoes) of light from different depth within biological tissue. A spectral-domain OCT (SDOCT) setup, illustrated in Fig. 2, was used to perform the imaging study. The SDOCT is based on a fiber-optic Michelson interferometer illuminated by a broadband source (BBS). The pigtailed output power of the BBS was ~ 12 mW; the central wavelength was at 1320 nm; and the full width half maximum (FWHM) of spectral bandwidth was ~ 90 nm, thus yielding a coherence length of $L_c \approx 8.5$ μm. The broadband light was split equally into the reference and sample arms of the Michelson interferometer. To guide the OCT scan, green light from a 532-nm diode laser was coupled into the input arm via a 95%:5% (at 1320 nm) fiber coupler. In the reference arm, a stationary mirror was employed to match the optical path lengths between the sample and the reference arms of the fiberoptic interferometer. The sample arm was connected to a bench-top stereoscope in which light exiting the fiber was collimated to $\phi 5$ mm, scanned laterally by a servo mirror, and focused by an $f = 40$ mm achromatic lens onto the rat-bladder surface under examination. In the detection fiber, the light returning from sample and reference arms was recombined and connected to a spectral radar in which it was collimated by a fiber-optic achromatic lens ($f = 55$ mm), diffracted by a holographic grating ($d = 1200$ mm^{-1}) and then focused by an achromatic lens ($f = 120$ mm) onto a 1024-pixel line InGaAs photodiode ar-

ray (pixel size: 25 μm) mounted on a motored 3-D stage for high-precision focus alignment. On the basis of the optical setup, the spectral radar covers ~ 110 nm spectral range with a spectral resolution of $\Delta\lambda \approx 0.11$ nm. According to Nyquist sampling criterion, the imaging depth of SDOCT system is determined[21] by $\Delta z_{Nq} = \lambda^2/(4\Delta\lambda) \approx 3.96$ mm (in free space, with $n = 1$). The detected spectral graph was amplified, digitized and streamlined to an image workstation via a 2-channel 12 bit A/D (DAQ6111E, NI) at 5 MHz to permit 2-D OCT imaging at nearly 8 fps (post image processing). Because the depth-resolved backscattering profile (A-scan) of a rat bladder was encoded in spectral interferogram at different modulation frequencies, Fourier transform was performed to reconstruct the image. Because of extensive data processing [e.g., spline interpolation, fast Fourier transform (FFT)] involved in converting spectral graphs to a reconstructed 2-D SDOCT image, instantaneous image processing and display was reduced to ~ 5 fps. Data processing to reconstruct each depth profile or A-scan was synchronized with scanning of the lateral servo mirror in the sample arm following detection of each spectral graph until a 2-D image is completed and displayed. The axial and the transverse resolutions of SDOCT were determined by the coherence length and the focal spot size of the OCT scope, respectively. On the basis of the above parameters used in our setup, the axial resolution of the reconstructed autocorrelation function [i.e., the axial point spread function (PSF) was $\Delta z_{OCT} \approx 8.9$ μm, which matched well with the theoretical result ($L_C \approx 8.5$ μm), as shown in Fig. 3]. The diffraction-limited transverse resolution was $\Delta r_{OCT} \approx 12$ μm, the field of view per OCT scan was $FOV_{OCT} \approx 6 \times 2$ mm (lateral/axial directions), and the measured system dynamic range[22,23] was ~ 111 dB.

HFUS imaging was performed with an ultrasonic microimaging system (Vevo 770, Visualsonics Inc., Toronto, Canada) using a single-element, 40 MHz $f/2$ probe (RMV 704) with a focal length of $f_{US} = 6$ mm. 2-D cross-sectional ultrasound B-mode (USB) imaging can be performed in real time (34 fps). The axial and lateral resolutions of the HFUS transducer were $\Delta z_{HFUS} \approx 40$ μm (in soft tissue) and $\Delta r_{HFUS} \approx 80$ μm, respectively, and the field of view per the HFUS

scan was $FOV_{HFUS} \approx 10 \times 10$ mm (lateral/axial directions). For *ex vivo* HFUS imaging performed in this study, the bladder specimens were immersed in PBS, which also served as the ultrasonic coupling media between the HFUS transducer and the bladder tissue under examination. Images were acquired with the region of the bladder specimens (e.g., mostly the urothelium or TCCs) centered at the focus. HFUS images were reviewed independently to ensure a double-blind study.

Sensitivity and specificity were calculated for both OCT and HFUS, in which histology served as the objective standard. The results of OCT and HFUS were classified as normal, inflammation, or TCC based on the backscattering and echo characteristics that differentiated rat-bladder morphology. More specifically, inflammation was diagnosed by OCT and in some cases by HFUS based on decreased backscattering or echo in the LP. TCC was diagnosed by OCT as urothelial thickening with enhanced urothelial heterogeneity or backscattering with drastically reduced penetration, and by HFUS as increased mass (e.g., outgrown lesions). Similarly, necrotic lesion was detected by OCT as extremely high backscattering with missing underlying structures, but exhibited low echo in HFUS. Normal urothelium and inflammatory lesions were considered negative ($-$) whereas TCC was considered positive ($+$). Chi-square analysis was performed to compare the sensitivity and specificity of HFUS and SDOCT to $p < 0.05$, considered statistically significant.

3 Result

Both OCT and HFUS detect bladder morphological features based on their backscattering differences optically or ultrasonically. Previous studies indicated that because of high resolution (e.g., $\sim 10 \ \mu$m), OCT delineated the urothelium (U) as a low scattering thin layer, the lamina propria (LP) as of high scattering, the muscularis (M) as of high scattering but showing large bifurcated structures, and in some cases the attached fatty layer (F) as barely resolved larger fat cells in a normal rat bladder. OCT was able to differentiate urothelial denudation, LP edema, urothelial hyperplasia, and TCC of rat bladder based on urothelial thickening and backscattering enhancement; however, staging of TCC was limited to T1 (not for major papillary lesions) because of limited imaging depth of OCT within the cancerous lesions, which often induced a drastic OCT signal drop. To compare to HFUS, a set of three cross-sectional images (i.e., OCT, HFUS, and histology) are presented for each lesion. All the originally 12-bit gray-scale cross-sectional images (6 mm lateral $\times 2.1$ mm vertical in bladder tissue) are displayed in pseudo color with no further postimage processing. All the originally 8-bit gray-scale HFUS images are displayed in pseudo color to enhance the visibility for different layers of rat bladder and are cropped to match the size of the corresponding OCT scans.

Figure 4 shows the results of a normal rat balder imaged by OCT (a) and HFUS (b) in comparison to histology (c). OCT delineated morphological details, such as the low-scattering urothelium ($51 \pm 5 \ \mu$m), the high-scattering lamina propria ($\sim 119 \ \mu$m), the muscularis ($\sim 29 \ \mu$m), and attached fat ($\sim 166 \ \mu$m), as well as the two blood vessels in the LP. The results compared favorably to the corresponding histology (U: $52 \pm 4 \ \mu$m, LP: $\sim 113 \ \mu$m, M: $\sim 322 \ \mu$m) except that the attached fatty layer (F: $\sim 10 \ \mu$m) shrunk substantially
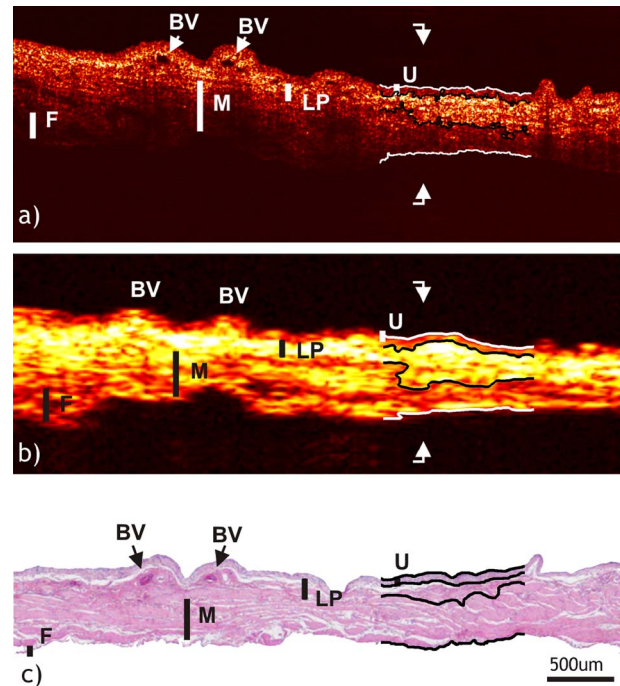
Fig. 4 (a) Normal rat bladder imaged by OCT, (b) HFUS, and (c) compared to histology. OCT delineated morphological details, such as the low scattering urothelium (U, $51 \pm 5 \ \mu$m), the high-scattering lamina propria (LP, $\sim 119 \ \mu$m), the muscularis (M, $\sim 296 \ \mu$m), and attached fat (F, $\sim 185 \ \mu$m), as well as two BVs in the LP. The OCT identifications compared favorably to the corresponding histology. HFUS was able to resolve urothelium (U, $66 \pm 11 \ \mu$m) as low echo and the underlying bladder layers similar to those of OCT (e.g., LP: echo high, M and F: echo lower). The traces in (a, b) were the interfaces of the segmented layers (e.g., U, LP, and M using image processing methods including despeckling, thresholding, and edge detection). Traces in (c) were the pathologist's manual segmentation.
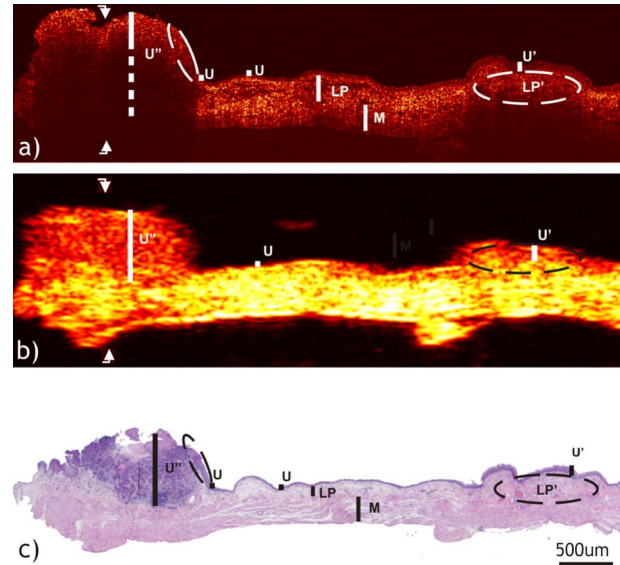
during tissue fixation. Surprisingly, HFUS (b) was able to resolve U ($66 \pm 11 \ \mu$m) as low ultrasonic scattering or low echo and the underlying bladder layers (LP: $\sim 123 \ \mu$m, M: $\sim 333 \ \mu$m, F: $\sim 222 \ \mu$m), similar to those of OCT identifications (e.g., LP: echo high, M and F: echo lower). As can be seen, the speckle patterns in the HFUS image are much larger than those in OCT image, especially in the transverse direction. As a result, the two small blood vessels (BVs) were not identified by HFUS imaging. Because of inherent speckle noise in OCT and HFUS images, accurate tissue differentiation (e.g., U, LP, and M) by computer image segmentation remains challenging, in particular, in areas such as lesions and folds that exhibit shadowing artifacts induced by either irregular surface or decrease in LP scattering. Nevertheless, computer segmentation in flat and normal areas of the rat bladder can be implemented, as shown Fig. 4. The following image processing methods were applied to segment bladder layers (U, LP, and M) in OCT (a) and HFUS (b) images: (*i*) both were converted to 8-bit grayscale images; (*ii*) low-pass Gaussian filtering with radius of 4 pixels was applied to minimize speckle noise; and (*iii*) edge detection to segment different bladder layers. To do this, the mean gray-scale value with standard deviation $M \pm \sigma$ of a small 5×50-pixel RIO within a layer such as U or M was sampled (e.g., $M_U = 74 \pm 15$
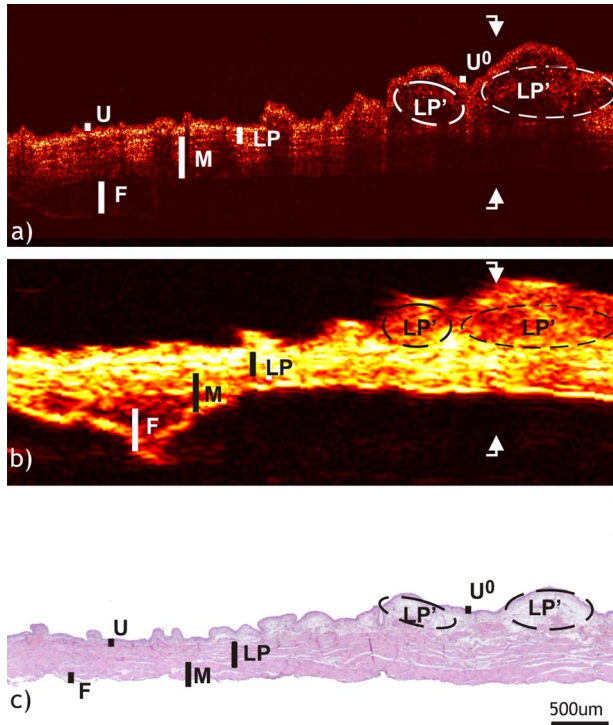
Fig. 5 Rat bladder undergoing acute inflammatory reaction. OCT (a) was able to image the morphological details of the bladder and detect two inflammatory infiltrates or edemas (LP′) in the lamina propria as confirmed by histology (c). HFUS (b) barely resolved the difference between LP and M. Although two lesions (LP′) were detected as echo low, the diagnosis was unspecific because it was unable to differentiate the thin urothelium U^0.

Fig. 6 Rat bladder with two lesions. OCT (a) diagnosed the left lesion as TCC (U″) and the right lesion as minor hyperplasia (U′), but failed to identify the attached urothelial hyperplasia (dashed circle) and to stage U″. HFUS (b) was able to stage the invasion of U″ as a T1 cancer but was unable to diagnose the right lesion because it failed to identify U′ and LP′.

$M_M = 50 \pm 10$ for U and M layers), and then the regions were extended to the surrounding pixels to form the contours (i.e., edge of the layer) using the thresholding values of $M \pm 2\sigma$ (e.g., $M_U = 74 \pm 30$, $M_M = 50 \pm 20$) where 2σ is the tolerance range, which takes into account of speckle-induced intensity fluctuations. Because of residual speckle noise or shadowing artifacts (e.g., surface folds), often a few contours were formed so that they had to be manually connected to form the entire layer. The histological image (c) was manually segmented based on pathologist's identification. It is noteworthy that further attempts of segmentation to the left region in image (a) and to the right side in both images (a) and (b) failed due to shadowing artifacts induced by the BVs and the folds, respectively.

Figures 5–8 represent four groups of *ex vivo* images of rat bladders at different stages of tumorigenesis following AY-27 cell instillation. Like the MNU cancer model,[24] the disease progression of this cancer model involves early acute chemical cystitis or injuries of the urothelium (e.g., acid wash during instillation), causing leakage of urine constituents or AY27 cells through disruptive bladder barriers, which begins a process of inflammatory reactions of the underlying LP and M layers and, in turn, causes fibrosis and urothelial malignancies (e.g., mostly due to AY27 cell growth). Therefore, the cancer model allows us to evaluate the potential of OCT and HFUS for visualizing the morphological alternations pertinent to the growth of bladder tumors, including edema, inflamma-

tion, ulceration, urothelial lesions, and the subsequent TCC invasion. Figure 5 shows the rat bladder undergoing acute inflammatory reaction. OCT (a) was able to image the morphological details (e.g., U, LP, M, and F) of the bladder and detect the underlying lesions as two inflammatory infiltrates or edemas (LP′), as confirmed by histology (c). HFUS (b), in this case, barely resolved the difference between LP and M, but detected the two lesions (LP′) as echo-low shadow. Because of swelling (LP′), this part of urothelium (U^0) above the lesions was considerably stretched thinner than the surrounding normal U. Unlike OCT that resolved it as a thin, low-scattering superficial layer (30–40 μm), HFUS failed to identify the thinning urothelium. It must be noted that the ability to identify U^0 is critical; otherwise, the large echo-low lesions might be misdiagnosed as TCCs by HFUS, as will be discussed below.
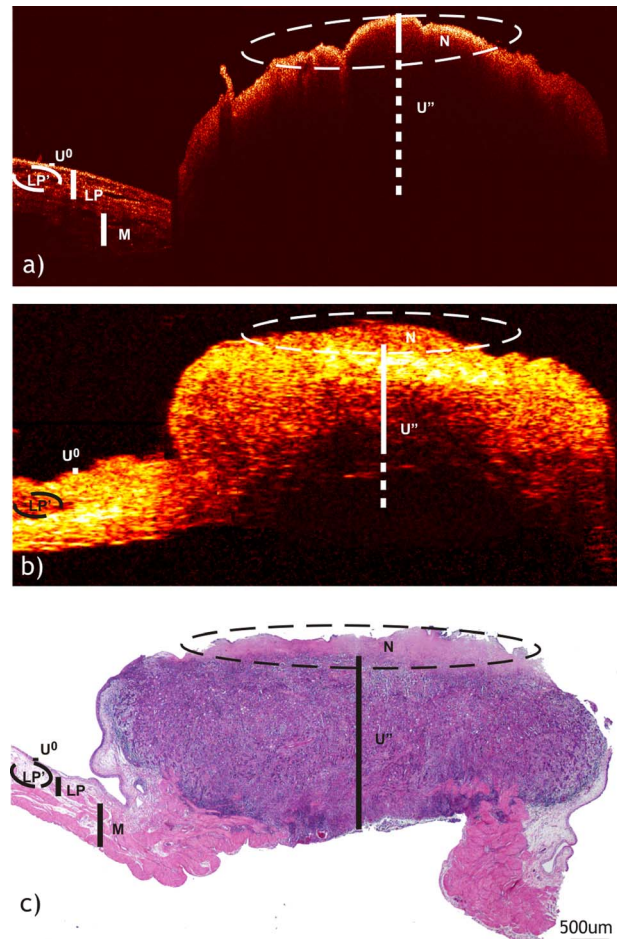
Figure 6 shows the results of a bladder containing two lesions. Based on enhanced urothelial backscattering ($V_{U''}V_U \approx 1.3$) and decrease of OCT signal below the surface, OCT (a) diagnosed the lesion on the left as TCC (U″). However, because of steep slope, OCT failed to identify the attached urothelial hyperplasic lesion over the TCC as highlighted by the dashed circle. For the right lesion, OCT was able to diagnose it as minor hyperplasia (U′) based on delineation of the low-scattering, slightly thickened but uniform urothelium (83 $\pm$ 10 μm). Unlike the inflammatory lesions in Fig. 5, the submucosal edema (LP′) was more severe with local vasodilatation as confirmed by histology (c), which led to missing underlying bladder structures in OCT image (a) as a result of enhanced blood-induced light attention.[24] In comparison, HFUS (b) was able to stage the invasion of U″ as a T1 cancer (622 $\pm$ 37 μm) that OCT failed (indicated by dash line). However, as HFUS was unable to differentiate U′ and
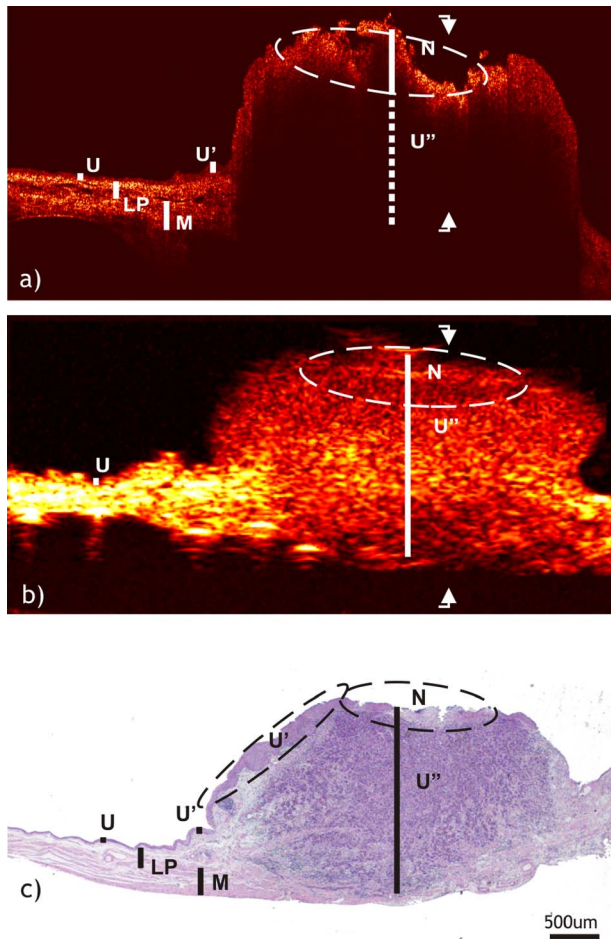
Fig. 7 Rat bladder with a large T2 tumor. OCT (a) was able to identify the boundary and the transition with a minor hyperplasia (U′), as well as the necrosis (N) above the large TCC (U″). Again, OCT failed to stage the tumor. HFUS (b) was able to stage it as a T2 tumor (U″), as confirmed by histology.

Fig. 8 Rat bladder with a high-grade T3 tumor. OCT was able to diagnose the lesion as TCC (U″) and detect the superficial necrosis (N). HFUS (b) failed to stage the tumor because of insufficient imaging depth. In contrast to OCT, necrosis showed low echo in HFUS. Unlike the T2 TCC in Fig. 7, the high-grade T3 TCC appeared echo high, possibly due to increased heterogeneity to enhance ultrasonic scattering.

LP′, the right lesion might be misdiagnosed as either an inflammatory lesion or a T1 TCC.

Figure 7 shows the results of a large T2 cancer. Because of limited penetration, OCT (a) was unable to stage the TCC (U″), whereas HFUS (b) could stage it as T2. At the left boundary, OCT could identify the minor hyperplasia (U′) which HFUS barely resolved. However, as indicated by the dashed circle, the large TCC (U″) was encapsulated by the hyperplasic urothelium (U′), causing the lesion not to show enhanced backscattering ($V_{U″}$) except at the center where the necrotic tissue as indicated by the dashed circle (N) exhibited increased scattering. On contrary, the necrotic lesion showed echo low in the HFUS image. Although this large TCC might be misdiagnosed by OCT as severe hyperplasia (i.e., urothelial thickening without backscattering enhancement), the abrupt decrease of the OCT signal within the lesion should differentiate it from hyperplasia. Figure 8 shows a more advanced high-grade T3 TCC. Similar to Fig. 7, the cancerous lesion was embedded under the urothelium as shown by histology (c). Therefore, no enhanced backscattering was observed in the OCT image (a) except in the area of the large

necrosis. As has been found in previous animal and clinical OCT studies, necrotic lesions tended to exhibit substantially enhanced backscattering ($>2.5\ V_U$). Again, HFUS (b) showed low echo in the necrotic lesion. However, possibly due to increased heterogeneity in the TCC (high grade) leading to increased ultrasonic scattering, the HFUS signal level dropped substantially along the depth of the lesion so that HFUS failed to stage the invasion of this T3 tumor. Interestingly, the urothelium adjacent to the large TCC was almost denuded ($U^0 \approx 19 \pm 2\ \mu$m) so that OCT barely detected the thin urothelium ($U^0 \approx 21 \pm 5\ \mu$m), but the HFUS measurement was overestimated ($U^0 \approx 65 \pm 10\ \mu$m) and appeared as normal. Both OCT and HFUS could identify the inflammatory lesion (LP′) underneath the denuded urothelium (U^0).

A total of 56 spots (i.e., sites) were imaged from 39 bladders, among which 7 lesions were confirmed as TCCs by histology. Both OCT and HFUS were able to identify these large lesions as TCCs. However, HFUS falsely identified 32 lesions that were detected by OCT and histology as benign inflammatory lesions. According to the results on a per lesion basis,

the sensitivity and specificity for OCT were each 100%; whereas for HFUS, they were 100 and 61%, respectively.

4 Discussion

Because of resolution limitations of current medical imaging techniques (e.g., X-ray, MRI), white-light cystoscopic *en face* imaging or cystoscopy following urine cytology is presently the clinical standard for diagnosis of bladder cancers and the recurrence following transurethral resection of bladder tumors (TURBT). Unfortunately, cystoscopy lacks depth resolution; it may miss flat TCCs (e.g., carcinoma *in situ*) and often relies on random biopsy for conclusive diagnosis, whose diagnosis depends on the selection of biopsied sites and results in insufficient diagnostic sensitivity and specificity, according to clinical statistics. OCT is a new enabling optical imaging technique that offers sub-10 μm spatial resolution and a superb signal-to-noise ratio. Our recent clinical study demonstrated that MEMS-based OCT cystoscopy has the potential to drastically enhance the sensitivity to 91% and specificity to 80% for noninvasive bladder cancer diagnosis.[11] However, the study also suggested limited usage of OCT for staging the invasion of large bladder cancers to T1 or less. Therefore, a more effective staging technique is desirable.

In this study, we compare two promising high-resolution imaging modalities (i.e., OCT and HFUS) for imaging urinary bladders and for diagnosing and staging bladder cancers. The research methodology that confirmed the OCT and HFUS identifications with the corresponding histology (i.e., gold standard for clinical diagnosis) allowed us to evaluate the potential of these two imaging techniques for future noninvasive clinical diagnosis of bladder cancers and their technical limitations. Moreover, the rat-bladder cancer model by AY-27 cell instillation provided a platform to enable systematic imaging identifications of the morphological changes induced by bladder tumorigenesis, such as edema, cystitis, hyperplasia, and urothelial carcinomas.

The results in Fig. 4 show that both OCT and HFUS were able to resolve the urothelium of a normal rat bladder as an echo-low thin layer. Figure 9 further compares the A-scans between these two imaging techniques at a lateral position highlighted by arrows in images Figs. 4(a) and 4(b). Apparently, the OCT measurement of U $\approx$ 51 $\pm$ 5 μm is accurate compared to the histological evaluation of U $\approx$ 52 $\pm$ 4 μm, whereas that of HFUS (U $\approx$ 66 $\pm$ 11 μm) can only be a rough estimate, as a result its axial resolution ($\Delta z_{HFUS} \approx$ 40 μm) is inferior to OCT ($\Delta z_{OCT} \approx$ 8.9 μm). Nevertheless, the ability to resolve urothelium is critical and may provide HFUS with the potential to diagnose urothelial cancers. Similar to Fig. 9, Fig. 10 compares the A-scans signal of OCT and HFUS over
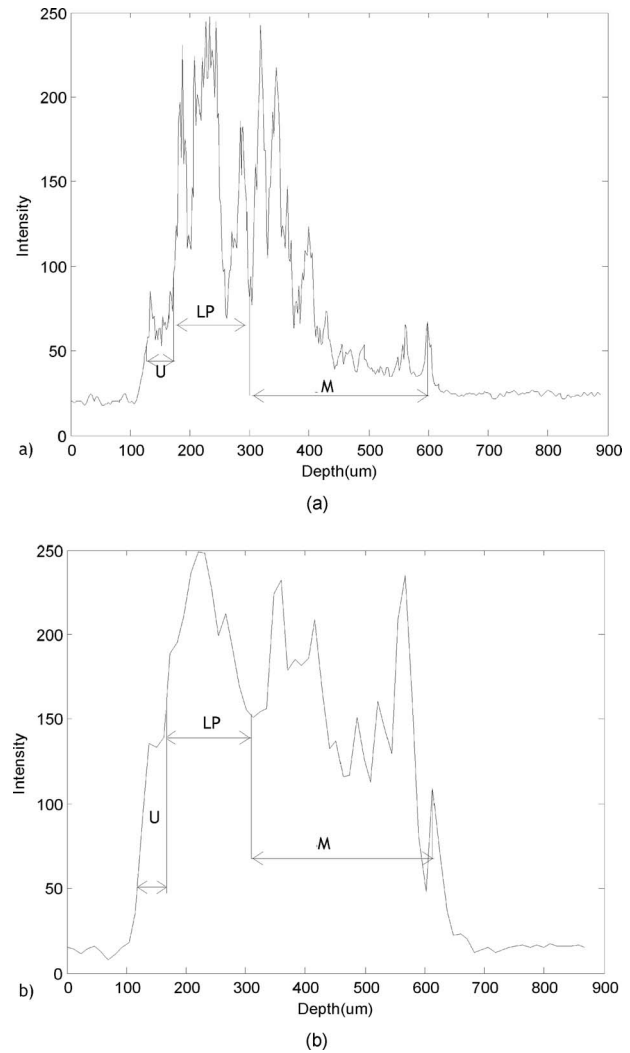

Fig. 9 A-scans of OCT (a) and HFUS (b) on normal bladder at a lateral position highlighted by a pair of arrows in Figs. 4(a) and 4(b). The OCT measurement of U $\approx$ 50 μm matched well with histological evaluation, whereas that of HFUS (U $\approx$ 60 μm) was a rough estimate.

an inflammatory lesion at the lateral position highlighted by arrows in images Figs. 5(a) and 5(b). On the basis of the signal changes in Fig. 10, OCT can identify the benign urothelium, whereas HFUS fail to identify the interface between the U and the underlying lesion in the LP, both of which exhibit low echo. This will seriously limit the diagnostic value of HFUS for bladder cancer detection, because both benign lesions, such as the inflammatory lesion (LP′) in Fig.

Table 1 TCCs staged by OCT and HFUS.

Tumor No.	1	2	3	4	5	6	7
OCT[a]	$\geq$T1	>T1	>T1	>T1	>T1	>T1	>T1
HFUS	T1	T2	T2	$\geq$T2	>T2	>T2	>T2
Histology	T1	T2	T2	T2	T3	T3	T3

[a]Because of limited imaging depth, OCT was unable to stage tumors beyond T1 and even outgrown T0 tumors.
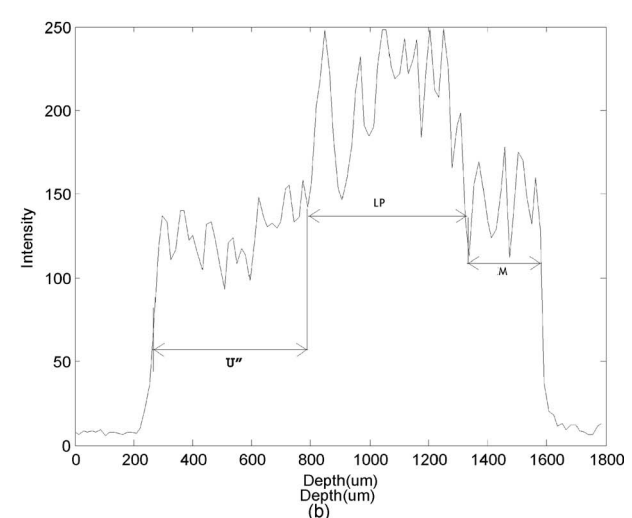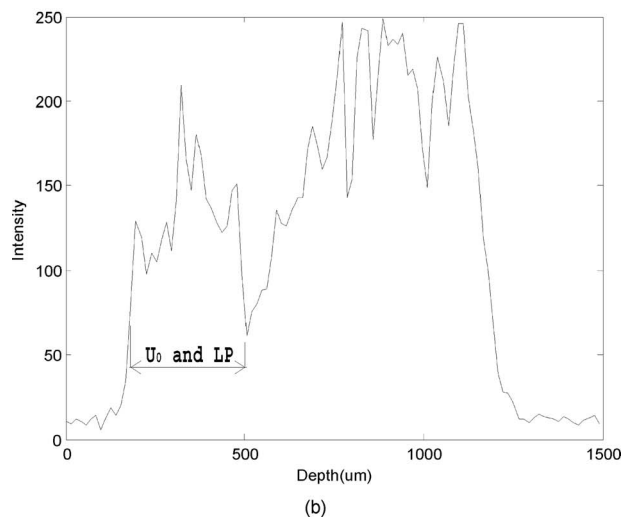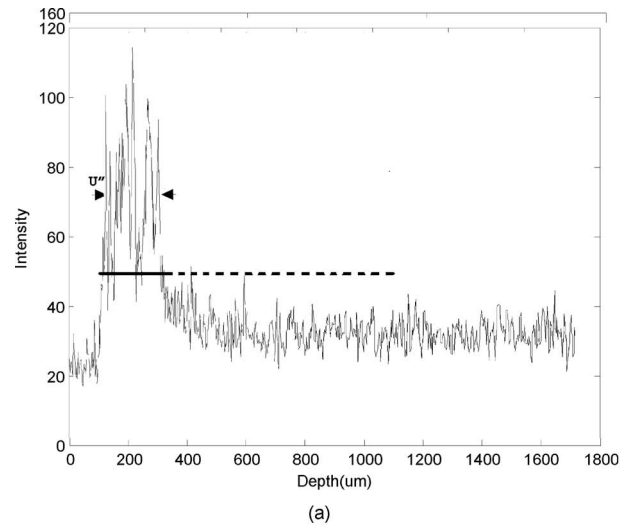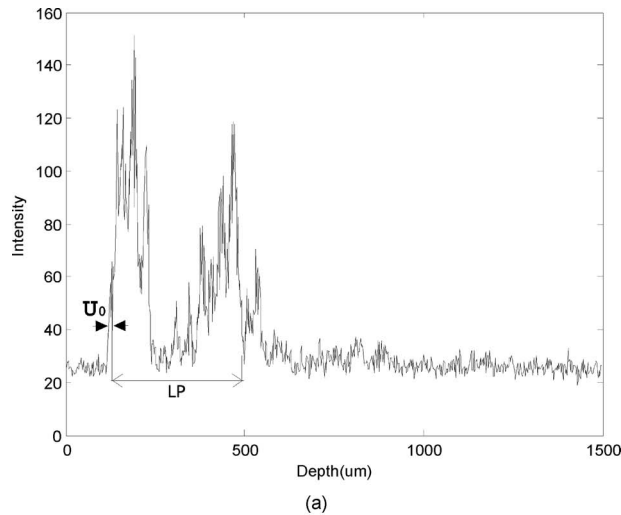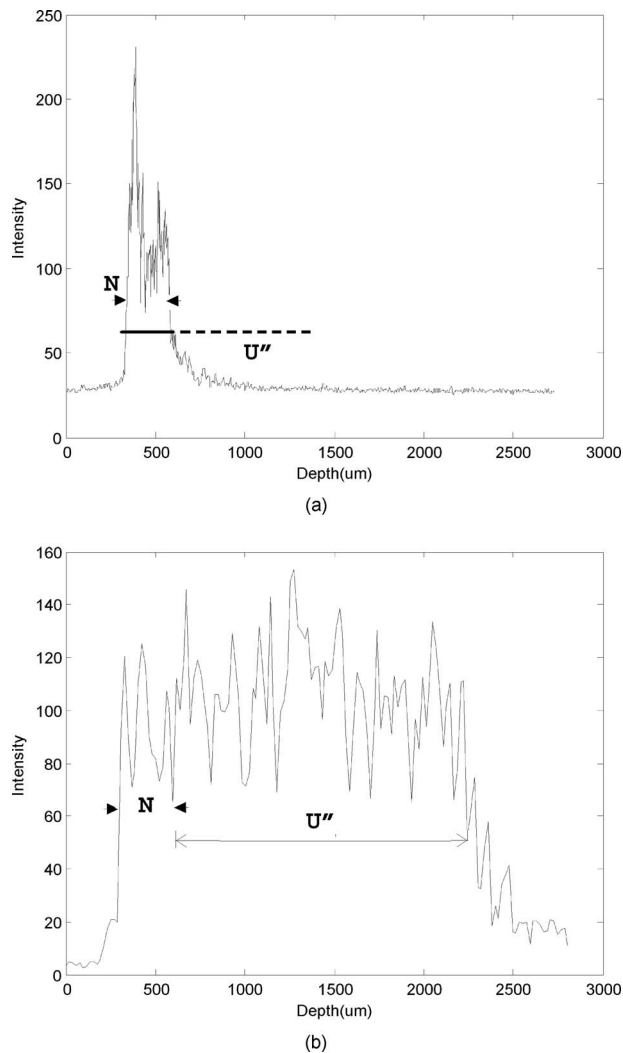
Fig. 10 A-scans of OCT (a) and HFUS (b) across an inflammatory lesion at a lateral position highlighted by a pair of arrows in Figs. 5(a) and 5(b). OCT identified the very thin urothelium ($U^0 \approx 18 \ \mu m$), which HFUS missed because both U^0 and the underlying lesion LP′ exhibited echo low.

Fig. 11 A-scans of OCT (a) and HFUS (b) across a T1 tumor at a lateral position highlighted by a pair of arrows in Figs. 6(a) and 6(b). OCT signal dropped to noise background within the first 200 μm and thus failed the tumor invasion, whereas HFUS measured the invasion to 540 μm and staged it as T1 tumor.

5 and the hyperplasia (U′) and LP edema (LP′) in Fig. 6, and malignant lesions, such as TCCs in Figs. 6 and 7 are echo low and therefore cannot be differentiated. However, despite the inability to differentiate these lesions, HFUS can precisely stage the invasions of these two large TCCs in Figs. 6 and 7. Figures 11 and 12 show the A-scans signal of OCT and HFUS over T1 and T2 tumors highlighted by arrows in Figs. 6(a), 6(b), 7(a), and 7(b), respectively, which OCT imaging fails to stage. Therefore, these two techniques can be combined to take advantage of their individual characteristics for bladder imaging (i.e., OCT for diagnosis and HFUS for staging of bladder cancers). It should also be noted that in many cases OCT and HFUS show similar contrasts for bladder components. For instance, both techniques show low backscattering/ echo for urothelium, muscularis, and fat, and high scattering/ echo for lamina propria. However, the image contrast of HFUS for bladder cancers may be different. For instance, the two TCCs in Figs. 7 and 8 appear as uniform and echo low,

whereas the high-grade TCC in Fig. 8 appears as less homogeneous and echo high at the top of the cancer. This could be attributed to the increased heterogeneity in high-grade TCCs. Also, on contrary to OCT, which drastically diminishes penetration, necrosis (which often exists on top of large high-grade TCCs) appears echo low and "transparent" (without substantive attenuation) in HFUS imaging.

In this study, all seven TCC lesions induced by AY-27 cancer model were diagnosed by both OCT and HFUS (100% sensitivity); however, these tumors were outgrown and thus likely identifiable via surface appearance. Although the specificity of OCT reached 100%, HFUS falsely identified 32 inflammatory lesions as TCCs, resulting in a reduced specificity of 61%, due to the fact that both TCCs and inflammatory lesions exhibited low echo so that HFUS failed to differentiate. With a 39% difference in specificity, Chi-test shows a significant enhancement of OCT over HFUS diagnoses. However, it is noteworthy that only 7 TCCs were yielded out of 39

(a)

(b)

Fig. 12 A-scans of OCT (a) and HFUS (b) across a T2 tumor at a lateral position highlighted by a pair of arrows in Figs. 7(a) and 7(b). OCT detected necrosis (N) but failed to stage the tumor whereas HFUS measured the full thickness (2.1 mm) of the tumor and staged it as T2.

AY27-cell-treated rats and all were all outgrown; the high diagnostic sensitivity/specificity may not necessarily reflect those of either clinical scenario or other animal TCC models (e.g., MNU or SV40-T transgenic mouse models). Results of our recent *in vivo* clinical study demonstrated both the potential and complexity endoscopic OCT for bladder cancer diagnosis.[11] Nevertheless, the study provides an interesting comparison between OCT and HFUS and demonstrates the potential of combining these two complimentary techniques to enhance the diagnosis and staging of bladder cancers. Table 1 summarizes the staging results of all seven TCCs by these two imaging modalities, where T0–T3 refer to tumors confined within U, invaded to LP, M, and beyond M.

5 Conclusion

Despite that the image fidelity (both contrast and resolution) of OCT is superior to HFUS, both techniques are able to delineate the morphological architectures of normal rat blad-der and exhibit similar image contrasts in terms of high or low backscattering or echo. OCT is able to diagnose inflammatory lesions, hyperplasia, and TCC based on urothelial thickening and urothelial backscattering or heterogeneity enhancement; however, its staging of bladder cancer invasion is limited to T0 and T1 due to limited penetration depth. In contrast, HFUS fails to differentiate some benign lesions and TCC, but it can stage the invasion of T2 TCC (to muscularis). Therefore, a multimodality approach combining OCT and HFUS may potentially enhance the diagnosis and staging of bladder cancers. In addition, because technological advances have permitted transurethral HFUS and endoscopic OCT, a cystoscopic approach combining these two image techniques may improve current urological examinations of bladder cancers and help to guide TURBT, in which both high-resolution imaging for diagnosis and deep penetration for tumor staging are desirable.

References

1. ACS (2006), ⟨http://www.cancer.org/downloads/STT/CAFF2006PWSecured.pdf⟩ *Cancer Facts & Figures 2006.*
2. R. S. Cajulis, G. K. Haines, D. Friashidvegi, K. Mcvary, and J. W. Bacus, "Cytology, flow-cytometry, image-analysis, and interphase cytogenetics by fluorescence *in-situ* hybridization in the diagnosis of transitional-cell carcinoma in bladder washes—A comparative-study," *Diagn. Cytopathol* **13**(3), 214–223 (1995).
3. M. F. Sarosdy, P. Schellhammer, G. Bokinsky, P. Kahn, R. Chao, L. Yore, J. Zadra, D. Burzon, G. Osher, J. A. Bridge, S. Anderson, S. L. Johansson, M. Lieber, M. Soloway, and K. Flom, "Clinical evaluation of a multi-target fluorescent *in situ* hybridization assay for detection of bladder cancer," *J. Urol. (Baltimore)* **168**(5), 1950–1954 (2002).
4. H. Leyh, M. Marberger, P. Conort, C. Sternberg, V. Pansadoro, F. Pagano, P. Bassi, L. Boccon-Gibod, V. Ravery, U. Treiber, and L. Ishak, "Comparison of the BTA stat (TM) test with voided urine cytology and bladder wash cytology in the diagnosis and monitoring of bladder cancer," *Eur. Urol.* **35**(1), 52–56 (1999).
5. D. Huang, E. A. Swanson, C. P. Lin, J. S. Schuman, W. G. Stinson, W. Chang, M. R. Hee, T. Flotte, K. Gregory, C. A. Puliafito, and J. G. Fujimoto, "Optical coherence tomography," *Science* **254**(5035), 1178–1181 (1991).
6. Z. P. Chen, T. E. Milner, D. Dave, and J. S. Nelson, "Optical Doppler tomographic imaging of fluid flow velocity in highly scattering media," *Opt. Lett.* **22**(1), 64–66 (1997).
7. J. F. deBoer, T. E. Milner, M. J. C. vanGemert, and J. S. Nelson, "Two-dimensional birefringence imaging in biological tissue by polarization-sensitive optical coherence tomography," *Opt. Lett.* **22**(12), 934–936 (1997).
8. U. Morgner, W. Drexler, F. X. Kartner, X. D. Li, C. Pitris, E. P. Ippen, and J. G. Fujimoto, "Spectroscopic optical coherence tomography," *Opt. Lett.* **25**(2), 111–113 (2000).
9. A. F. Fercher, C. K. Hitzenberger, G. Kamp, and S. Y. Elzaiat, "Measurement of intraocular distances by backscattering spectral interferometry," *Opt. Commun.* **117**(1-2), 43–48 (1995).
10. B. Povazay, K. Bizheva, A. Unterhuber, B. Hermann, H. Sattmann, A. F. Fercher, W. Drexler, A. Apolonski, W. J. Wadsworth, J. C. Knight, P. S. J. Russell, M. Vetterlein, and E. Scherzer, "Submicrometer axial resolution optical coherence tomography," *Opt. Lett.* **27**(20), 1800–1802 (2002).
11. C. S. D. L. Z. Wang, W. Waltzer, J. Liu, H. Xie, and Z. Yuan, "*In vivo* Bladder Imaging with MEMS-based endoscopic spectral domain optical coherence tomography," *J. Biomed. Opt.*, **12**(2), 034009_1–8 (2007).

12. P. R. Malone, J. Westonunderwood, P. M. Aron, K. W. Wilkinson, A. E. A. Joseph, and P. R. Riddle, "The use of transabdominal ultrasound in the detection of early bladder-tumors," *Br. J. Urol.* **58**(5), 520–522 (1986).

13. M. Koraitim, B. Kamal, N. Metwalli, and Y. Zaky, "Transurethral ultrasonographic assessment of bladder-carcinoma—Its value and limitation," *J. Urol. (Baltimore)* **154**(2), 375–378 (1995).

14. S. Tanaka, S. Yoshida, H. Okanobu, S. Oka, N. Manabe, S. Nagata, T. Hiyama, M. Ito, Y. Kitadai, M. Sumii, M. Yoshihara, and K. Chayama, "Clinical usefulness of high-frequency ultrasound probes (HFUP) for new invasion depth diagnosis in submucosal colorectal carcinoma," *Gastrointest. Endosc.* **56**(4), S146–S146 (2002).

15. D. A. Fishman, L. Cohen, S. V. Blank, L. Shulman, D. Singh, K. Bozorgi, R. Tamura, I. Timor-Tritsch, and P. E. Schwartz, "The role of ultrasound evaluation in the detection of early-stage epithelial ovarian cancer," *Am. J. Obstet. Gynecol.* **192**(4), 1214–1221 (2005).

16. D. H. Char, G. Kundert, R. Bove, and J. B. Crawford, "20 MHz high frequency ultrasound assessment of scleral and intraocular conjunctival squamous cell carcinoma," *Br. J. Ophthamol.* **86**(6), 632–635 (2002).

17. M. Vogt, A. Knuttel, K. Hoffmann, P. Altmeyer, and H. Ermert, "Comparison of high frequency ultrasound and optical coherence tomography as modalities for high resolution and non invasive skin imaging," *Biomed. Tech.* **48**(5), 116–121 (2003).

18. A. Das, M. V. Sivak, A. Chak, R. C. K. Wong, V. Westphal, A. M. Rollins, J. Willis, G. Isenberg, and J. A. Izatt, "High-resolution endoscopic imaging of the GI tract: a comparative study of optical coherence tomography versus high-frequency catheter probe EUS," *Gastrointest. Endosc.* **54**(2), 219–224 (2001).

19. P. Patwari, N. J. Weissman, S. A. Boppart, C. Jesser, D. Stamper, J. G. Fujimoto, and M. E. Brezinski, "Assessment of coronary plaque with optical coherence tomography and high-frequency ultrasound," *Am. J. Cardiol.* **85**(5), 641–644 (2000).

20. Z. Xiao, T. J. McCallum, K. M. Brown, G. G. Miller, S. B. Halls, I. Parney, and R. B. Moore, "Characterization of a novel transplantable orthotopic rat bladder transitional cell tumour model," *Br. J. Cancer* **81**(4), 638–646 (1999).

21. M. Wojtkowski, R. Leitgeb, A. Kowalczyk, T. Bajraszewski, and A. F. Fercher, "*In vivo* human retinal imaging by Fourier domain optical coherence tomography," *J. Biomed. Opt.* **7**(3), 457–463 (2002).

22. S. H. Yun, G. J. Tearney, B. E. Bouma, B. H. Park, and J. F. de Boer, "High-speed spectral-domain optical coherence tomography at 1.3 um wavelength," *Opt. Express* **11**(26), 3598–3604 (2003).

23. Z. G. Wang, Z. J. Yuan, H. Y. Wang, and Y. T. Pan, "Increasing the imaging depth of spectral-domain OCT by using interpixel shift technique," *Opt. Express* **14**(16), 7014–7023 (2006).

24. T. Q. Xie, M. L. Zeidel, and Y. T. Pan, "Detection of tumorigenesis in urinary bladder with optical coherence tomography: optical characterization of morphological changes," *Opt. Express* **10**(24), 1431–1443 (2002).